Measurement Science
and Technology

PAPER

Characterization of absolute cavity radiometers for traceability to SI of solar irradiance

To cite this article: J L Balenzategui *et al* 2022 *Meas. Sci. Technol.* **33** 115009

IOP Publishing Measurement Science and Technology
Meas. Sci. Technol. **33** (2022) 115009 (15pp) https://doi.org/10.1088/1361-6501/ac849d

Characterization of absolute cavity radiometers for traceability to SI of solar irradiance

J L Balenzategui[1,*], J de Lucas[2], J Cuenca[1], A González-Leiton[1], M Molero[1], F Fabero[1], J P Silva[1], E Mejuto[1], R Muñoz[3], A Arce[3] and E Prieto[3]

[1] CIEMAT, Departamento de Energía, Laboratorio de Energía Solar Fotovoltaica (PVLab), Avenida Complutense, 40–28040 Madrid, Spain
[2] INTA, Centro de Metrología y Calibración (CMyC), Laboratorio de Temperatura y Humedad. Ctra. Ajalvir, Km 4–28850 Torrejón de Ardoz, Madrid, Spain
[3] CEM, Área de Longitud e Ingeniería de Precisión. C/Alfar, 2. 28760 Tres Cantos, Madrid, Spain

E-mail: jl.balenzategui@ciemat.es

Received 4 April 2022, revised 1 July 2022
Accepted for publication 27 July 2022
Published 12 August 2022

Abstract

Solar-type cavity radiometers are instruments of the highest metrological level for measuring solar direct normal irradiance. To ensure their traceability and performance, they are periodically compared to the World Group of Standards, which realizes the World Radiometric Reference (WRR), in the International Pyrheliometer Comparisons (IPCs). Additionally, they can be characterized in an absolute way, with direct traceability to SI units and with their measurement uncertainty calculated. This paper describes the different techniques and procedures applied for the characterization and calibration of solar cavity radiometers, with the main results obtained to date in the case of an Automatic Hickey–Frieden (AHF) radiometer. Voltmeters, resistors, temperature sensors and the area of the precision apertures have been calibrated, while the effective absorptance, temperature coefficients, optical scattering and non-equivalence factor have been evaluated. The temperature dependence of the electrical current in the cavity heater has also been analysed. The resulting corrections obtained for the AHF by characterization are compatible with the WRR factors obtained by this instrument in the past IPCs. An uncertainty of 0.42% ($k = 1$) has been obtained, and this paper discusses further improvements that may be able to reduce this figure to the desired expanded uncertainty of $U = 0.1\%$ ($k = 2$).

Keywords: absolute radiometer, solar radiometry, solar irradiance, metrology, calibration, pyrheliometer, traceability

(Some figures may appear in colour only in the online journal)

1. Introduction

Solar radiation is the most influential energy source for Earth's climate system and its energetic balance. It is measured and studied (through several physical magnitudes) in fields of science such as astronomy and space physics, medicine, agriculture, architecture, or climatology and meteorology. It is, of course, the primary energy source for solar thermal and photovoltaic conversion systems.

Scientific community is carrying out a huge effort for understanding the mechanisms governing Earth's climate, and are demanding a higher accuracy from experimental data and from climatic models [1, 2]. In this sense, *Earth radiation budget* (ERB) and *surface radiation budget* are considered as essential climate variables (ECVs) by the Global Climate Observing System (GCOS) [3]. These ECV variables are

* Author to whom any correspondence should be addressed.

obtained from measurements in space of the total solar irradiance (TSI) and of the irradiance (both long- and short-wave) emitted or reflected by the Earth's surface and atmosphere. GCOS and others also pointed out the importance of a continuous recording of solar irradiance and posed basic requirements for its measurement: 1 W m^{-2} in absolute accuracy and 0.3 W m^{-2} per decade in stability [4, 5]. For reference, last accepted value of solar irradiance at the mean Earth–Sun distance (1 au), the *solar constant*, is ∼1361 W m^{-2} [6–8] so that figure-of-merit implies getting an uncertainty better than 0.075% in TSI measurements (≈1/1361, 735 × 10^{-6}). The same figure would represent around ∼0.1% at ground-level (for 1000 W m^{-2} reference irradiance). Requirements suggested two decades ago by National Institute of Standards and Technology (NIST) researchers [9, 10] for space radiometers were even more demanding: spectral radiation reflected from Earth's surface be measured with an accuracy of 0.2%, spectral solar irradiance with 0.1% and TSI up to 0.01%. The same degree of accuracy of 0.01% for TSI was suggested in the ASIC3 community workshop held in 2007 [2, 11].

Obviously, adequate instrumentation is necessary to meet these requirements. In recent years, there have been many technical developments in solar radiometry, revealing an impressive dedication for its correct assessment with increasing accuracy, and the key importance of these measurements along decades. Evolution of instruments and scales in solar irradiance radiometry can be found in the literature [12–17].

Currently, the device used as reference for the measurement of the solar direct normal irradiance (DNI) at ground level, and of the TSI and ERB in space, is a so-called *absolute cavity radiometer* (ACR) [12, 18, 19]. First ACR versions were developed in the JPL-NASA at the end of the 1960s [20, 21] and were conceived for supporting space measurements of TSI and ERB. A comprehensive compilation of different generations of cavity radiometers launched in satellites for TSI and ERB measurement purposes and their uncertainties can be found elsewhere [11, 22]. Adaptations of these space ACRs were readily applied for on-ground measurement of solar irradiance [23–25] and are nowadays the pyrheliometers of the highest metrological level in the solar irradiance scale. ACRs are considered, under certain conditions, as *primary* reference standards by the World Meteorological Organization (WMO) CIMO Guide [26] and as Class AA instruments in the ISO 9060:2018 Standard [27].

However, from a strict metrological perspective, these on-ground solar-type ACRs can be considered (with a few exceptions) neither as *absolute* nor as *primary* instruments.

Cavity radiometers work under the *Principle of electrical substitution, Principle of electrical compensation*, or *Principle of equivalence* [28, 29], so radiant power becomes directly linked to electrical power, which is more easily and accurately measured. However, despite their careful construction, the realization of that *Principle* is not perfect and a number of uncertainty sources of a systematic nature (due to optical, radiative, electrical and thermal effects) can deviate the radiometer from that ideal behaviour.

Absolute responsivity and/or its deviation from the ideal *Principle* can be determined by two means: (a) the calibration by comparison against a reference standard, or (b) the complete characterization of the instrument. This is illustrated in figure 1.

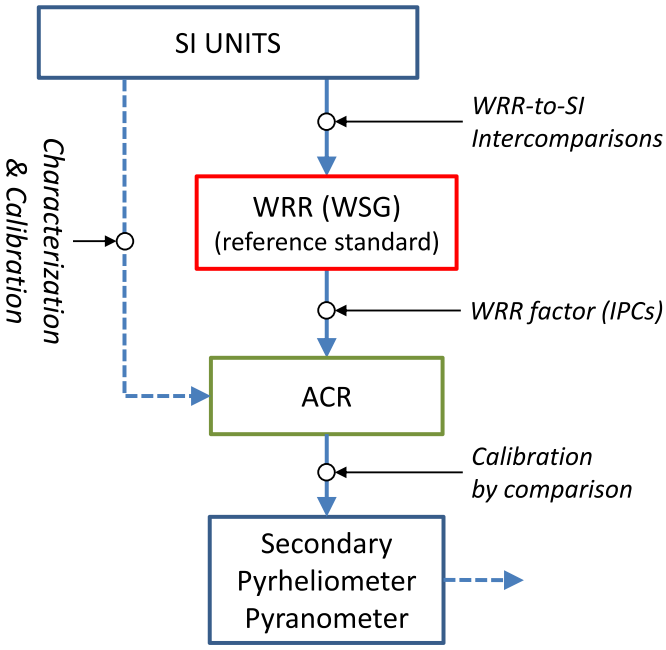

Figure 1. Schematic chart showing the two possible ways for getting traceability to SI units of solar irradiance measurements by an ACR, as described in the main text.

In the field of solar irradiance radiometry, the first method is more suitable due to its greater simplicity, this is, the *direct comparison* of the ACR to another standard reference cavity radiometer under natural sunlight in outdoor conditions [26]. Nowadays, the traceability of solar ACRs to SI is usually obtained by their comparison to a special group of cavity radiometers [18, 30], the World Standard Group (WSG), designated by WMO to realize or materialize the World Radiometric Reference (WRR). Traceability to WRR (ideally) provides direct traceability to SI, which has been periodically verified through intercomparisons between WRR and SI radiometric scales [31–34]. A deviation of 0.3% is usually applied to account for the difference or shift between scales [34, 35].

Although the WRR is based on an 'artifact' or 'prototype', it is designated and recognized by consensus as the primary reference of solar irradiance, and every radiometer in WSG is considered as the practical realization (*mise en practique*) of the 'solar' W m^{-2} unit. Hence, WMO promotes the International Pyrheliometer Comparisons (IPCs) every 5 years, in which ACRs from institutions all around the world are compared to WSG. These IPCs are held in the Physikalisch-Meteorologisches Observatorium Davos (PMOD)/World Radiation Center in Davos (Switzerland), which was designated by WMO to maintain the WSG. The IPC serves to disseminate WRR scale, to ensure uniformity in measurements of solar irradiance at a global level, and also to check stability of the WRR itself.

As a result of IPCs, a WRR *transfer factor* is assigned to each participating instrument (with an associated σ standard

deviation and the number N of valid values), this is, a factor of deviation from the WRR reference. This transfer factor is used as a correction constant by the ACR user to reproduce the irradiance values that WSG would have given in the same location and operating conditions. The WRR scale is later disseminated from ACRs to secondary reference devices, working standards and field sensors, in a hierarchical sequence [17, 36].

Therefore, as a consequence of their comparison to a primary reference (WSG), these ACRs become *secondary* standard instruments from a metrological point of view. In fact, WMO regulations argues these ACRs can still be designated and used as primary reference instruments *only if* some specifications are fulfilled [18, 26], but can be used as a secondary standard when they are merely calibrated by comparison to the WSG.

Alternatively or complementarily, a solar ACR can also be subjected to *characterization* [18, 33, 37], the second method mentioned above. That is, to undergo a set of laboratory calibrations, independent tests, modelling or numerical simulation of its individual components and correction factors, identifying and quantifying the sources of individual uncertainties in the measurements, and calculating the total uncertainty of the instrument [38]. Characterization was considered from the very moment of defining the WRR as a requirement for the absolute radiometers in order to determine their accuracy and reliability [18]. Thus, a complete characterization makes the radiometer become a 'true' *absolute* instrument [19] in the sense that its solar irradiance values (and their uncertainty) are directly traced to fundamental SI units, and to be *primary* [39] because it does not require it does not require reference or comparison to another ACR to get that traceability (although comparisons to other primary instruments are convenient, required or advisable).

Examples of characterization of solar ACRs can be found in the literature, although such characterizations are mainly performed by the own designers and manufacturers of each model of instrument [37, 40–57]. Of key importance have been the characterization and calibration of solar radiometers used in space missions involved in the measurement of TSI and ERB, because of the discrepancies found in the irradiance measured by different generations of instruments and spacecraft [2, 7].

However, ACR versions adapted for ground-level operation have rarely been characterized, especially for the commercial ACR versions, and even less frequently by independent laboratories [58–60]. In practice, it is very difficult for a laboratory not involved in the design or engineering of an ACR to face the task of its characterization. The technical complexity of the characterization is very high (even considered risky because of the delicate manufacture of the cavities) and it is generally considered not worth doing it. However, characterization is necessary and provides interesting and important information for an in-depth understanding of the properties of a particular instrument, needed to establish its uncertainty associated with systematic effects, to determine the origin of deviations from the ideal *Principle*, and to analyse options for improvement.

Figure 2 schematically shows the process of metrological characterization of an ACR, similar to that of any other

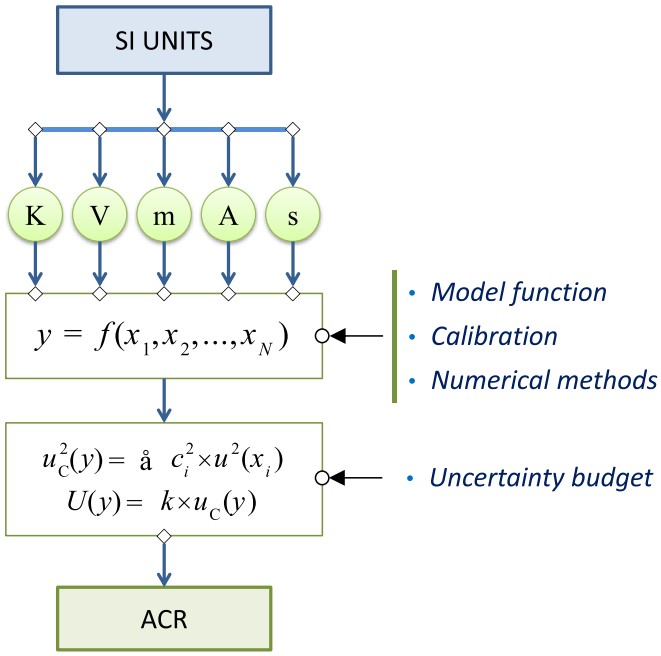

Figure 2. Diagram of the characterization process of an ACR according to the approach described in this work. Every model of ACR has a particular model function whose input variables are linked to one or several SI units. This has been suggested by means of the symbols K, V, m, A, s, which stand for the SI units of temperature, voltage, length, electrical current and time. U, u_C, c_i, k are uncertainty types, coefficients and coverage factor used in the uncertainty evaluation (see section 4).

measuring instrument. In brief, it should be based on a *measurement model function* (MMF), $y = f(x_1, x_2, \ldots, x_N)$, which relates the magnitude y to be determined with some input variables (measured during its operation) and a set of known parameters (characteristic constants of the instrument), and not containing empirical factors [61]. In the particular case of ACRs, guidelines for their characterization and recommended parameters to take into account were already suggested by WMO CIMO-VII more than 40 years ago [62].

Therefore, the characterization task involves, on the one hand, the calibration of the measuring instruments used by the ACR to obtain solar irradiance (e.g. a multimeter measuring current and voltage). And, on the other hand, the determination or estimation of the characteristic parameters: some of them might be directly measured or calibrated (e.g. the area A of a precision aperture), while other could require modelling, simulation, or numerical computation, or even a mixture between indirect measurements and modelling. Calibration of input quantities links them to SI units by means of reference standards (to units of temperature, current, voltage, area, etc).

Each input quantity x_i has to be determined with an associated uncertainty $u(x_i)$ and a sensitivity coefficient c_i with which its contribution to the standard uncertainty of y is accounted for, generally expressed as a *quadratic sum:* $u_C{}^2(y) = \sum[c_i{}^2 \cdot u^2(x_i)]$ in the case of uncorrelated input quantities [63]. These sensitivity coefficients c_i are derived from the MMF $y = f(x_1, x_2, \ldots, x_N)$ as $c_i = \delta f/\delta x_i$. However,

to our knowledge, this approach of using an explicit MMF has not been applied to date in the characterization of ACRs and, in general, only a quadratic sum of uncertainty contributions, $u_C{}^2(y) = \sum[u^2(x_i)]$, supposing all $c_i = 1$, has been used. The latter would be valid when all the parameters and input quantities involved in the MMF are multiplicative factors (as in [62]), but it is not clear that all the radiometer's operational equations follow that structure. Therefore, the method described here can be considered as a generalization of the procedure of characterization, which would be suitable for any type of solar radiometer based on an arbitrary MMF, and it is one of the original contributions of this work.

Although this research task can be very challenging, PVLab-CIEMAT, in close collaboration with INTA, has been working in the characterization of two commercial-type solar ACRs: an Automatic Hickey–Frieden (AHF) radiometer [41], manufactured by Eppley Labs (USA), and a PMO6 radiometer [37], now manufactured by Davos Instruments (CH). These radiometers constitute the reference for the calibration of PVLab solar irradiance secondary standards.

This paper describes the application of these general principles of characterization based on MMF to the case of the AHF radiometer and the results obtained so far. It has been carried out from the perspective of a R&D laboratory specialized in the field of solar energy, which uses ACRs as (*primary*) reference standards for the calibration of solar sensors, but which has not taken part in the design or manufacture of the instrument. First, basics about the AHF radiometer and its MMF are given. After, the different techniques and procedures for evaluating each input quantity in the MMF are explained. Next, the uncertainty budget is evaluated, according to the individual contributions and sensitivity coefficients derived from the MMF. Finally, further steps for improving the current value of the standard uncertainty $u \cong 0.42\%$ are discussed.

Although some of the methods described here could be common to other works on this field, there is a lack of information in the literature about the characterization of AHF parameters and about their uncertainty. Besides, some improvements of particular application for this radiometer (as an alternative method for determining of the non-equivalence factor, or the addition of a resistance thermometer in AHF control box allowing for dynamic temperature corrections) are introduced in this work. Some results obtained during earlier phases of this research have been shared in conferences [64, 65].

2. Fundamentals of Eppley's AHF radiometer

2.1. AHF structure and operation

The HF is a cavity radiometer originally developed by J R Hickey and R G Frieden at the Eppley Labs in the mid-1970s for the Nimbus satellite series [41]. First terrestrial versions were commercially available in 1977 [23]. In 1978, three HFs already participated in the New River Intercomparison of Absolute Cavity Pyrheliometers NRIP-1 [66], and in 1980, there were six HF radiometers in the IPC-V intercomparison [67]. In 1985, WMO CIMO-IX decided to include an HF radiometer in the WSG [68] and by the IPC-VII [69] the HF 18478 was considered as a member of the WSG, still active today. Automatic versions (AHF) were developed in the early 2000s. By 2015, there were almost 50 AHFs/HFs taking part in the IPC-XII [30].

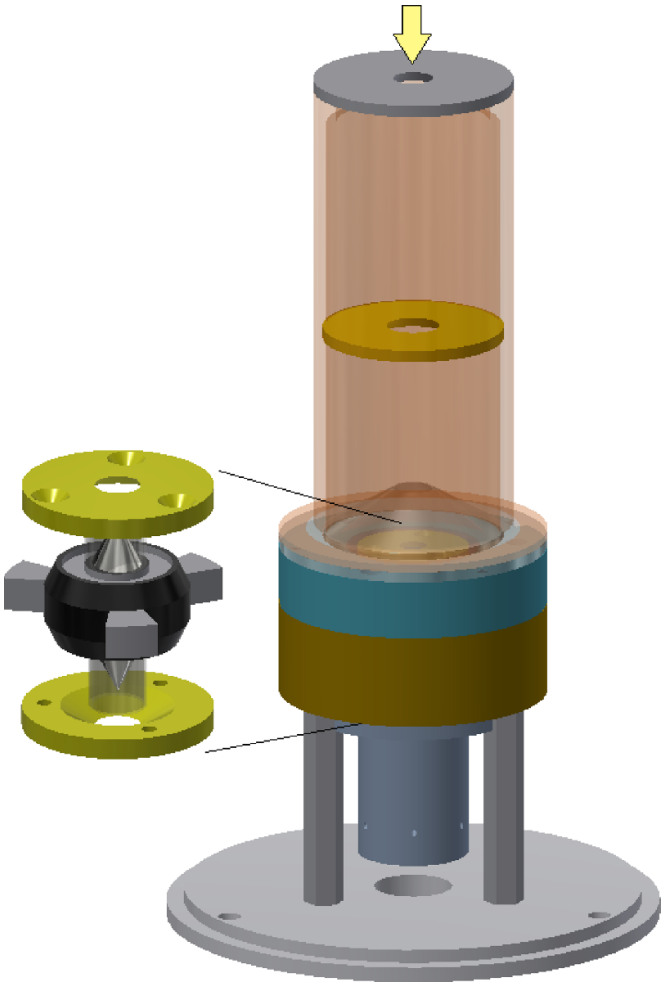

Figure 3. Three-dimensional model of the AHF radiometer (false coloured). On the left, the sensor formed by the twin cavities attached to the wire-bound thermopile and the precision apertures; in the cavities, the external cylinder has been made transparent to see the shape of the inner cone. On the right, internal view of the collimator tube and its baffles, the block containing cavities and thermopile, and the rear blackbody. The sensor on the left is not at scale. The yellow arrow on top shows the entrance aperture for radiation. There is an external tube fixed to the bottom plate (not shown in this view).

The sensor of the AHF consists of two twin cavities attached to opposite sides of a wire-bound thermopile wrapped in a toroidal structure (see figure 3). The rear cavity is open to a blackbody-like hollow aluminium block at ambient temperature, while the front cavity receives sunlight. This creates a balanced or compensated detector [41]. Geometry of the cavities is of the type cylinder-inner-cone, they are made of silver foil and internally coated with Chemglaze (Aeroglaze) Z302 black glossy paint.

The heater wire is internally wound in the cone and partially in the cylinder, in order to reproduce radiative heating distribution and amount (and a better equivalence between electrical and radiative heating). The cavity heater is connected in a four-wire Kelvin scheme, and heater voltage V_H and current I_H are measured with an external Agilent 34970A data-logger to calculate the electrical power P_E.

Sunlight reaches the front cavity through a collimator tube which reduces the field of view up to 5°, and a precision aperture of known area A. The front cavity is periodically occluded from sunlight by means of an electromechanical shutter integrated into an external protecting tube. During shutter closed phases (so called *calibration phase*) the cavity is only electrically heated and the voltage output V_{TE} of the thermopile is measured, as well as the thermopile offset signal V_{T0} when the cavity is not subjected to any excitation. During open phases, the cavity is only exposed to the sun radiative power (without any electrical heating) and the voltage output V_{TS} of the thermopile is measured every 30 s. This mode of operation corresponds to a *passive-type* radiometer. In normal operation, the calibration phase (lasting 2–3 min) is carried out every 30 min.

The ensemble of thermopile and apertures is placed inside a thick cylinder made of gold plated copper, which serves as support structure and as high thermal inertia heat sink. The collimator is fixed on one side of this thick block and the aluminium blackbody on the opposite side, thus defining which is the front cavity is and which is the rear one, although the sensor would ideally be reversible.

2.2. AHF measurement function

Operational equations of the radiometer can be found elsewhere [41, 47] but are compiled here for completeness. The fundamental working principle of the AHF is based on the linear dependence of *emf* generated in the thermopile on any of the excitation power sources (radiant, electrical). Output signal from this thermopile is, in theory, independent of the ambient temperature due to its symmetric compensating construction. Therefore, we can write these linear dependences as:

$$\begin{cases} V_{TS} - V_{T0} = k_S \cdot P_S \\ V_{TE} - V_{T0} = k_E \cdot P_E \end{cases} \tag{1}$$

where k_S, k_E are proportionality constants (the slopes of straight lines relating V_{TS} with P_S and V_{TE} with P_E).

On the one hand, the radiant power reaching the cavity would be given by:

$$P_S = A \cdot \alpha_C \cdot \gamma \cdot E \tag{2}$$

where E is the DNI, α_C is the effective absorptance of the cavity and γ is a *stray-light factor* associated to the collimator and baffles. Ideally, values of α_C and γ parameters would be 1.

On the other hand, electrical power delivered to the heater is calculated by:

$$P_E = I_H V_H - I_H^2 R_C = \frac{V_I}{R_N}\left(V_H - \frac{V_I}{R_N} R_C\right) \tag{3}$$

where heater current I_H is obtained from the voltage drop V_I in a shunt of resistance R_N, and the small power loss in the thin wires connecting the cavity heater to the circuit is estimated from their resistance R_C.

According to the *Principle of Electrical Substitution*, if excitation powers (radiant, electrical) are equivalent or indistinguishable to the effect of heating the cavity, the response of the system will be the same. In that case:

$$\frac{V_{TS} - V_{T0}}{P_S} = \frac{V_{TE} - V_{T0}}{P_E} \quad \rightarrow \quad k_S = k_E. \tag{4}$$

However, it is admitted that the practical realization of the principle can be somewhat imperfect. For example, due to different contributions of radiative, convective and conductive heat transfer under dissimilar power sources (electrical, radiant). This non-equivalence is also influenced by small manufacturing defaults, variability of material properties, aging, degradation, etc. Therefore, slight differences can be produced in the system output when exposed to these excitations, so then:

$$k_S \neq k_E \quad \rightarrow \quad L = k_E / k_S. \tag{5}$$

Being L named the *non-equivalence factor*, whose value ideally should also be 1 for a *perfect* equivalence between radiative and electrical powers.

Finally, combining equations (2)–(5), the solar irradiance is calculated from the AHF as:

$$E = \frac{L}{A\,\alpha_C\,\gamma} \cdot \left(\frac{V_{TS} - V_{T0}}{V_{TE} - V_{T0}}\right) \cdot \frac{V_I}{R_N}\left(V_H - \frac{V_I}{R_N} R_C\right). \tag{6}$$

This is the MMF of the AHF cavity radiometer, making irradiance E explicitly dependent on 11 input variables: $E = f(A, L, \alpha_C, \gamma, V_{TE}, V_{TS}, V_{T0}, V_H, V_I, R_N, R_C)$. In this function, operative type input variables (electrical signals measured during operation of the radiometer V_{TE}, V_{TS}, V_{T0}, V_H, V_I) and characteristic parameters (A, L, α_C, γ, R_N, R_C), ideally constant, can be identified.

Sometimes the correction parameters are grouped and referred to as the *calibration factor* of the radiometer:

$$C_F = \frac{L}{A \cdot \alpha_C \cdot \gamma} \tag{7}$$

whose ideal value would be $C_F \approx 1/A$. In the case of AHF, $A \sim 50$ mm^2 and therefore $C_F \sim 2 \times 10^4$ m^{-2}.

Additionally, during closed-phases, the AHF control system also calculates a parameter called *sensitivity* S (responsivity) of the instrument as:

$$\frac{1}{S} = C_F \cdot \frac{1}{V_{TE} - V_{T0}} \cdot I_H\,(V_H - I_H R_C). \tag{8}$$

So later, during open-phases, irradiance is simply obtained by computing:

$$E = \frac{V_{TS} - V_{T0}}{S}. \tag{9}$$

Values of sensitivity S are around 11 μV W^{-1} m^{-2} in normal outdoor operation of this radiometer.

3. Characterization of Eppley's AHF

As a starting point, it is necessary to identify which parameters in equation (6) can be subject of direct calibration, which ones need determination through modelling, and those requiring mixed or combined measure-calculation procedures.

A priori, input variables corresponding to electrical signals should allow external calibration. In general, components or parts of an ACR measurement system are not always easily accessible and usually cannot be disassembled for calibration without altering their properties. In the particular case of AHF, the output signals from thermopile (V_{TE}, V_{TS}, V_{T0}), heater voltage (V_H) and voltage drop in the shunt resistance (V_I) are externally measured by an Agilent 34970A data-logger. This logger also measures temperatures of two thermistors, one placed in the reference block and the other in the wall of the collimation tube. Thus two separate calibrations of the data-logger have been carried out, both for voltage and for temperature readings.

On the other hand, the shunt resistor R_N placed in the instrument control box and the parasitic resistance R_C of the wires up to the heater have been calibrated by independent tests. Further details about R_N characterization and its thermal drift are given later. The area of the precision apertures were calibrated by the Centro Español de Metrologia (CEM), the Spanish NMI, as described below.

However, the rest of parameters (L, α_C, γ) are much more difficult to be characterized, and a combination of experimental measurements and simulation has to be applied. The techniques and solutions found for the determination of the non-equivalence factor L and of the effective absorptance α_C are also described in the next sections. Determination of optical quality factor γ is still under way, as well as some other optical characterizations, and results will be disseminated elsewhere.

3.1. The area of the precision aperture

Precision apertures of an AHF consist in a chamfer circular hole about 8 mm in diameter, carefully drilled in a 4 mm thick disk made of invar (a 36% Ni/64% Fe alloy). Their shape can be seen in figure 3 (left). Nominal aperture area is 50 mm^2. Invar combines a great mechanical strength with a very low thermal expansion coefficient ($\sim$1–2 $\times$ 10^{-6} K^{-1} at ambient temperatures) [70].

The area of both apertures were calibrated in the Laboratory of Length and Precision Engineering of the CEM. The first approach was based on the measurement of the radius r by means of a vision machine with a resolution of 0.1 μm (Mitutoyo Ultra Quick Vision 350 Pro) with traceability to SI. A total of 360 points distributed along the perimeter of the opening were resolved (see figure 4). They were later approximated by a circumference fitted using least-squares, which gives the radius and the location of the centre. The method is of interest because it allows determining the degree of deviation in roundness. The value obtained for

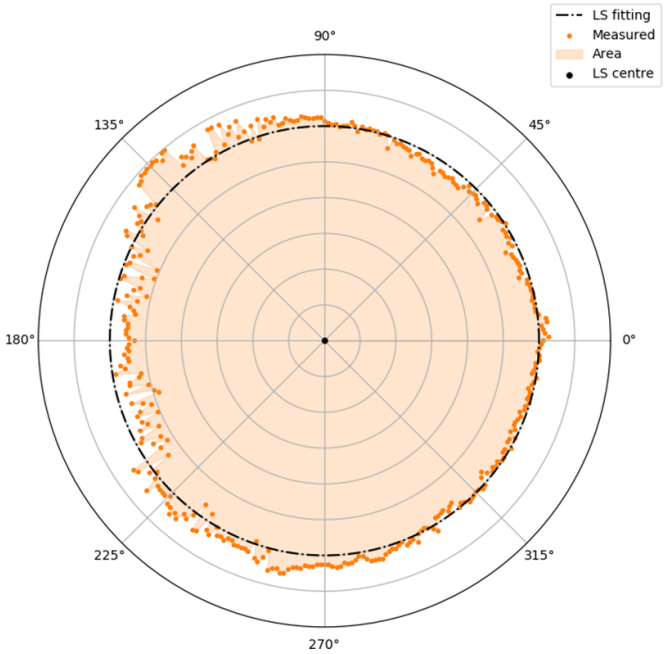

Figure 4. Determination of the area of the precision aperture (front cavity) of the AHF. A triangle is built from each couple of contiguous measured points and the least-squares centre. The total area is calculated by adding up the individual areas of all possible triangles.

the radius at a room temperature of (20 $\pm$ 0.5) °C was r = (3.997 $\pm$ 0.003) mm (k = 2). This would result in a calculated area of A = (50.1901 $\pm$ 0.0753) mm^2 (k = 2). However, the uncertainty obtained with this method was considered too large ($U \approx 0.15\%$ for k = 2) for the purpose of the AHF characterization.

For this reason, a different approach was applied on the basis of the same set of measured points to avoid the influence of the shape deviation on the radius uncertainty. The area was directly determined by adding the surfaces of the triangles created between two consecutive points measured in the border of the aperture and the centre of the circumference calculated by the least-squares fitting in the previous step. This method is equivalent to that applied by Physikalisch-Technische Bundesanstalt for circular apertures of radiometric applications [71]. The new value of the area so calculated was A = (50.183 $\pm$ 0.015) mm^2 (k = 2). Thus, uncertainty is now around $U = 0.03\%$ (k = 2) which is much more admissible for the objectives of this research, although there is still room for future improvements. Noticeably, this value of area is about 0.39% higher than that originally calculated by using the data provided by the manufacturer (7.978 mm diameter, given with no uncertainty).

3.2. The non-equivalence factor L

As a subtle difference with respect to other radiometers, the *Principle of electrical substitution* in AHF system is realized in terms of *equal power* instead of *equal temperature* (or equal

thermal flux) between open (radiant) and closed (electrical) phases. During closed phases, the control unit feeds the heater circuit with a voltage V_S calculated from the (last measured) radiant solar power P_S as:

$$V_S = \sqrt{R_H \cdot P_S} + (R_N + R_R + R_C)\sqrt{P_S/R_H} \qquad (10)$$

where the voltage drop in all the in-line (series connected) resistances is accounted for, with R_R being a relay resistance. Once the circuit is polarized with V_S and stabilized, the value of V_{TE} is measured, next the circuit is not powered for measuring offset V_{T0}, and then the sensitivity S of the radiometer is calculated.

Although slight differences between electrical and radiant power are experimentally detected, this approach works fine thanks to the extremely linear dependence of thermopile output voltage on any of the excitation powers. In fact, it is easy to probe that calculating sensitivity S in equation (8) would be equivalent to determining the slope k_E in equation (1), as $k_E \equiv S \cdot C_F$. Linearity of thermopile output at different (electrical) power levels (V_S from 0.1 V to 3.0 V) and temperatures (range 8 °C–50 °C) has been tested in the PVLab with the aid of a Fluke 5520A calibrator.

Given this behaviour and the particular realization of the *Principle*, it was suggested [64] that the non-equivalence factor L could be calculated directly from its definition equation (5), the responses of the thermopile to the two independent excitations could separately be analysed and the k_S, k_E slopes be calculated from the relationships in equation (1).

There are still some conceptual issues about how these independent excitations have to be realized for this purpose and how the thermopile response has to be measured for each excitation (for avoiding possible correlations). The approach currently applied in this research is based on the measurements of the AHF radiometer recorded in the last IPC-XII (2015), in which this instrument took part. WRR reference irradiance values E_{WRR} are independently measured during the IPC campaign by PMOD by the group of WSG standards while AHF system is synchronously measuring the thermopile output ($V_{TS} - V_{T0}$), so this allows calculation of k_S. WRR irradiance has been converted into solar power P_S as $P_S = A \cdot E_{WRR}$ by using the AHF aperture area calibrated by CEM. At the same time, measurements of the ($V_{TE} - V_{T0}$) output at different P_E powers were carried out by AHF system in the closed-phases along the same IPC, and were used there for calculation of its sensitivity S, so these values allow now the calculation of k_E. Notice that, this way, determination of k_S, k_E is based on data taken subsequently in the same period and working conditions.

Figure 5 shows the result of fitting linear models, implicit in equation (1), to these sets of experimental data. As observed, thermopile output is perfectly linear with power in the range of irradiances and working conditions during IPC-XII campaign. Numeric values of the k_S, k_E constants and their expanded uncertainties, calculated by Monte Carlo method [72], as

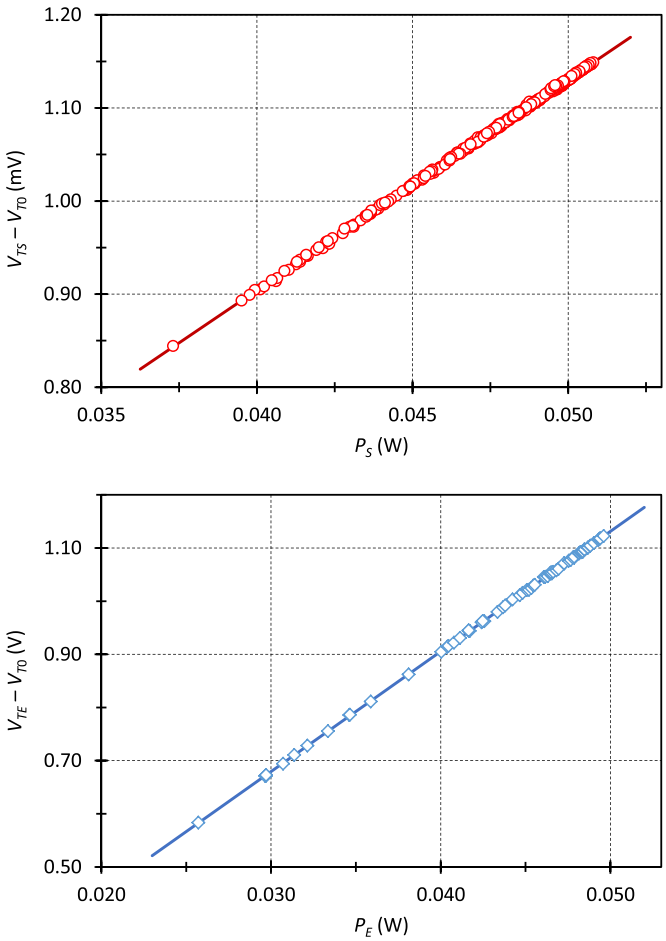

Figure 5. Calculation of the k_S, k_E constants in equation (1) (slopes of linear fits) for computing the non-equivalence factor L.

Table 1. Results of the determination of the k_S, k_E constants and of the non-equivalence factor L. Uncertainties of k_S, k_E have been calculated by the Monte Carlo method.

Parameter	Value	Uncertainty ($k = 2$)
k_S (mV W^{-1})	22.607 46	0.102 90 (0.46%)
k_E (mV W^{-1})	22.610 52	0.032 01 (0.14%)
L	1.000 135	0.004 768 (0.48%)

well as the final L factor obtained through equation (5), are collected in table 1.

As expected, the value of the non-equivalence factor is close to 1, and the difference with the value originally given by the manufacturer ($L = 1.0005$) is of only ~0.04%. However, there is no information about how the manufacturer's value and its associated uncertainty, were calculated.

However, the expanded uncertainty $U(L)$ obtained in this case is somewhat larger than desired. $U(L)$ seems to be mostly affected by the contribution into $U(k_E)$ and $U(k_S)$ of the uncertainty of the measurements of thermopile signals (V_{TE}, V_{TS}, V_{T0}) made by the data-logger. Further work will be necessary for a reduction of this contribution, not only at a technical level

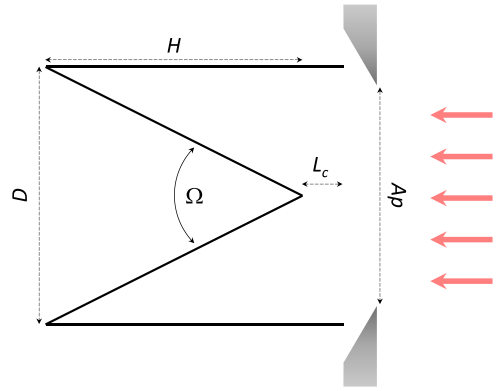

Figure 6. Sketch of the cavity behind the aperture area, and the geometrical parameters used for computation of the effective absorptance.

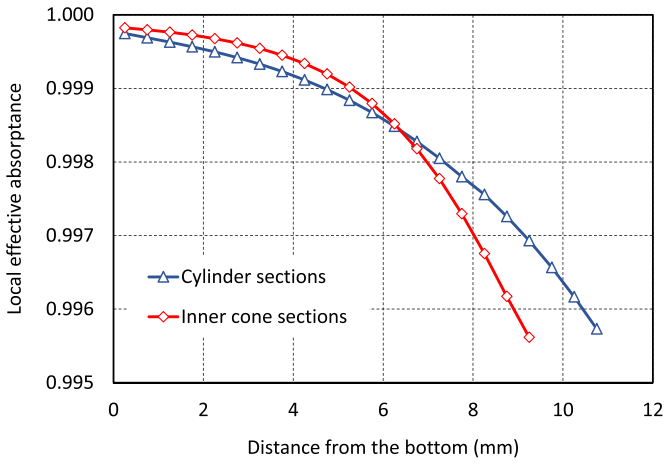

Figure 7. Local effective absorptance calculated for different sections of the cone and the cylinder. Distances are measured from the bottom of the cavity and assigned to the middle point of the section.

but also from the point of view of the concept applied for its estimation. As later discussed in section 5, the current procedure seems to make L dependent on the reference scale used for determining the optical power of the light source (WRR in this case).

3.3. *The effective absorptance α_C of the cavity*

As said, the cavity of AHF radiometer is of cylinder-inner-cone type, this is, the cone is oriented towards inside the cavity. Both the shape and the optical properties of the Z302 coating determine the absorptance α_C of the cavity. Figure 6 shows a sketch of the cavity and the parameters defining its dimensions.

Effective integrated normal absorptance has been calculated by the method of sums [73] by considering that all the solar radiation reaches the cavity only in direction parallel to its optical axis through the precision aperture (placed normal to this axis). For this method, the cylinder and the cone are divided into sections of equal length, normal to the optical axis, and local values of effective absorptance are calculated in each.

Intrinsic reflectance ρ of the Z302 paint can be assumed having specular ρ_S and diffuse ρ_D components, given by: $\rho = \rho_S + \rho_D = 0.05 + 0.01$ [28]. Then, since the specular contribution is five times larger than the diffuse one, it has been supposed that reflected radiation in each section can have two contributions: (a) one of diffuse type, which assumes that after the first initial reflection in the cone, radiation can either exit from the cavity through the aperture or be totally absorbed by the walls of the cylinder section, without additional reflections; and (b) another of specular type, which assumes that the light beam keeps this specular behaviour in successive bounces. It is easy to probe that, after five consecutive internal reflections, almost all the specular contribution is absorbed.

Finally, α_C is calculated by integration from the local values of irradiance over the cone in the region being illuminated by sunlight. Results of the local effective absorptance so calculated are shown in figure 7.

Uncertainty $U(\alpha_C)$ was obtained by the Monte Carlo method too [72] by varying in small amounts the geometrical parameters (figure 6) as well as the reflectance of the cavity, and assuming probability distributions of rectangular type for the input variables. Then, a final value of $\alpha_C = (0.999\ 12 \pm 0.000\ 11)$ was obtained for a coverage probability of 95%. The effective absorptance so calculated is similar to the experimental values obtained by independent measurements in AHF cavities at NIST [59]. At the same time, our calculations improve the accuracy of the value of α_C given by the manufacturer in the fact sheet of the instrument ($0.999 \pm 0.1\%$). Results have also been confirmed by numerical simulations of the reflectance of the cavity carried out in Zemax Optics Studio [65].

3.4. *Shunt resistance R_N and its dependence on temperature*

A wire wound power four-terminal axial PLV2 shunt resistor is used for measuring the current I_H supplied to the AHF cavity heater. It is placed within the control unit of the instrument, and has nominal values of $R_N = 10\ \Omega$ (with a tolerance of $\pm 0.01\%$), max rated power of 2 W and a temperature coefficient of $\pm 15 \times 10^{-6}\ ^\circ\mathrm{C}^{-1}$. Two different experiments were carried out for characterizing this shunt resistor: first, a high accuracy calibration of the resistance value; and second, determination of its actual temperature coefficient in the normal range of operating conditions inside the control box, thus allowing for dynamic corrections of sensitivity to temperature.

The shunt resistor was calibrated at a room temperature of $(23 \pm 1)\ ^\circ\mathrm{C}$ under a current intensity of 17.5 mA. This level of current was selected by considering the statistical distribution of electrical powers supplied into the heater resistance R_H during calibration phases in normal operation of the radiometer. Notice that, at this level of current, the shunt resistor is only dissipating around 3 mW so self-heating effects are negligible.

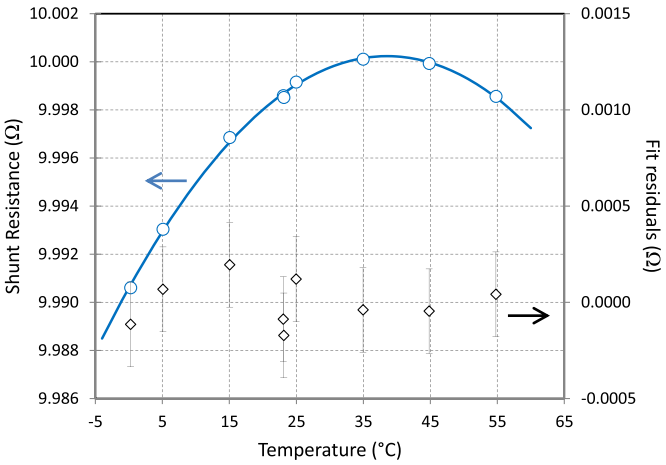

Figure 8. Experimental dependence of shunt resistance R_N on room temperature (empty circles; left axis). Solid line represents the fitting of these data points to a 2nd order polynomial. Fit residuals are also included (rhombuses; right axis).

The value of R_N so determined was $R_N = 9.998\ 69\ \Omega$ with an expanded uncertainty $U = 0.000\ 11\ \Omega$ ($k = 2$).

For the second purpose, a platinum resistance thermometer (PRT) Pt100 was integrated within the control unit in the proximity of the shunt. This Pt100 connected to the 34970A datalogger, as a whole (direct reading thermometer), was first calibrated by comparison to standard platinum resistance thermometers, traceable to the International Temperature Scale of 1990 [74], in controlled temperature baths. The maximum uncertainty was in this case $U = 0.01\ °C$ ($k = 2$).

A test for measuring the T coefficient of the shunt was later performed in the range from 0 °C to 55 °C inside a climatic chamber, by allocating temperature reference standards near the Pt100 shunt. Readings of the resistance R_N during the test were carried out with a standard HP 3458A multimeter. The results of this test are shown in figure 8.

As it can be seen, results confirm that thermal coefficient is quite low ($+35 \times 10^{-6}\ °C^{-1}$ in the range 0 °C–25 °C) and data points fit well to a 2nd order polynomial. Error bars shown with the fit residuals represent the expanded uncertainty ($k = 2$) obtained.

Finally, although their temperatures are not directly required for calculations with the model function equation (6), the two thermistors placed in the reference block and in the collimation tube were calibrated in the same climatic chamber (with temperature readings done by the datalogger). These mainly serve for monitoring of reference working conditions.

3.5. *Calibration of wires' resistance* R_C

The wires' resistance R_C was carefully measured by means of a calibrated Keysight 34420A micro-ohmmeter (resolution of $7\frac{1}{2}$ digits, range 1 Ω, test current 10 mA), with the cavity open in the laboratory at a room temperature of (25 ± 2) °C. The test wires were contacted in a four-point configuration with paired in-line Accuprobe tips (K-type Z-adjustable probe tips, reference IK2C8C3D). Total resistance was computed as the sum of the resistance of every branch (from positive contact point to cavity, and from cavity to negative contact point).

A total resistance of $R_C = (50.9907 \pm 0.0067)\ m\Omega$ ($k = 2$) was obtained as result. This value differs significantly from that of $R_C = 0.066\ \Omega$ originally given by the manufacturer (without uncertainty), which is commonly used in most of the HF/AHF radiometers as a default value [30], although the impact of this difference is about ∼0.1 W m^{-2} as maximum in terms of DNI irradiance.

4. Evaluation of uncertainty

One of the key aspects of characterization, as posed in the introduction, is the calculation of the uncertainty associated to the measurements of the radiometer. According to the JCGM 100:2008 or *GUM* guide [63], the combined standard uncertainty $u_C(y)$ of any magnitude y (output quantity), not directly measured but calculated by a measurement function $y = f(x_1, x_2, \ldots, x_N)$ from the values $x_1, x_2, \ldots, x_N$ of some other input quantities, is obtained by the expression:

$$u_C^2(y) = \sum_{i=1}^{N} \left[\frac{\partial y}{\partial x_i}\right]^2 u^2(x_i). \tag{11}$$

In the case of uncorrelated input quantities, or:

$$u_C^2(y) = \sum_{i=1}^{N} \left[\frac{\partial y}{\partial x_i}\right]^2 u^2(x_i) + 2\sum_{i=1}^{N-1}\sum_{j=i+1}^{N} \frac{\partial y}{\partial x_i}\frac{\partial y}{\partial x_j} u(x_i, x_j). \tag{12}$$

For correlated input quantities, where $u(x_i)$ is the standard uncertainty of the input quantity x_i and $u(x_i, x_j)$ is the estimated covariance of every pair (x_i, x_j). The partial derivatives are the called *sensitivity coefficients* c_i. Uncertainty $u(x_i)$ contribution of each input variable can be estimated either by statistical methods (analysis of series of repeated observations, named A-type estimation) or by means other than statistical (e.g. based on manufacturer's specifications, data provided in calibration certificates, etc, named B-type estimation).

Sometimes it is more convenient to calculate the *relative* standard uncertainty by dividing any of the preceding expressions (11) and (12) by the value of the magnitude under evaluation. For this purpose, assuming covariance terms can be neglected (no correlation among input variables), relative $u_C(y)$ will take the form:

$$\frac{u_C^2(y)}{y^2} = \frac{1}{y^2}\sum_{i=1}^{N} \left[\frac{\partial y}{\partial x_i}\right]^2 u^2(x_i). \tag{13}$$

In our case, by applying equation (13) to the measurement function equation (6), the relative uncertainty $u_C(E)/E$ of

each DNI irradiance value determined by the AHF radiometer would be calculated as:

$$\frac{u_C^2(E)}{E^2} = \frac{1}{E^2}\left[\frac{\partial E}{\partial L}\right]^2 u^2(L) + \frac{1}{E^2}\left[\frac{\partial E}{\partial A}\right]^2 u^2(A) + \ldots \frac{1}{E^2}\left[\frac{\partial E}{\partial \gamma}\right]^2 u^2(\gamma) + \frac{1}{E^2}\left[\frac{\partial E}{\partial \alpha_C}\right]^2 u^2(\alpha_C) + \ldots \frac{1}{E^2}\left[\frac{\partial E}{\partial V_{TE}}\right]^2 u^2(V_{TE}) + \frac{1}{E^2}\left[\frac{\partial E}{\partial V_{TS}}\right]^2 u^2(V_{TS}) + \ldots \frac{1}{E^2}\left[\frac{\partial E}{\partial V_{T0}}\right]^2 u^2(V_{T0}) + \frac{1}{E^2}\left[\frac{\partial E}{\partial V_H}\right]^2 u^2(V_H) + \ldots \frac{1}{E^2}\left[\frac{\partial E}{\partial V_I}\right]^2 u^2(V_I) + \frac{1}{E^2}\left[\frac{\partial E}{\partial R_C}\right]^2 u^2(R_C) + \ldots \frac{1}{E^2}\left[\frac{\partial E}{\partial R_N}\right]^2 u^2(R_N). \quad (14)$$

Calculating the partial derivatives and dividing by E^2 as given in equation (6), the final expression for $u_C(E)$ is:

$$\frac{u_C^2(E)}{E^2} = \frac{1}{L^2}u^2(L) + \frac{1}{A^2}u^2(A) + \frac{1}{\gamma^2}u^2(\gamma) + \ldots \frac{1}{\alpha_C^2}u^2(\alpha_C) + \frac{u^2(V_{TE})}{(V_{TE}-V_{T0})^2} + \frac{u^2(V_{TS})}{(V_{TS}-V_{T0})^2} + \ldots \frac{(V_{TS}-V_{TE})^2}{(V_{TE}-V_{T0})^2(V_{TS}-V_{T0})^2}u^2(V_{T0}) + \ldots \frac{1}{\left(V_H - \frac{V_I}{R_N}R_C\right)^2}\left[u^2(V_H) + \left(\frac{V_I}{R_N}\right)^2 u^2(R_C) + \ldots \left(V_H - 2\frac{V_I}{R_N}R_C\right)^2 \cdot \left(\frac{u^2(V_I)}{V_I^2} + \frac{u^2(R_N)}{R_N^2}\right)\right]. \quad (15)$$

The key aspect to be highlighted here is that uncertainty contribution of all input variables $u(x_i)$ in equation (15) are weighted by their corresponding sensitivity coefficients. Moreover, notice that addends in which electrical input variables are involved (V_{TE}, V_{TS}, V_{T0}, V_H, V_I) are dependent on operating conditions. During the calibration process of an irradiance detector, this implies that the full data set (within the accepted range of DNI irradiances, usually $E \geqslant 700$ W m^{-2}) has to be explored for calculating a representative value for $u_C(E)/E$. The common practice in laboratories is using either the largest uncertainty of the set (a worst-case approach, most conservative), or the value obtained at some reference conditions (for example, an irradiance of 1000 W m^{-2}). An alternative is to apply Monte Carlo methods for uncertainty calculation [72]. In this work, average values of these signals (measured in several calibration campaigns) have been used in order to have a first estimate of $u_C(E)/E$ (see table 2) that can also be used for future reference.

By using the results obtained during AHF characterization, taking the average values of (V_{TE}, V_{TS}, V_{T0}, V_H, V_I) as representative, and calculating the sensitivity coefficients in equation (15) for these values, a final figure of relative standard uncertainty $u_C(E)/E = 4224 \times 10^{-6}$ is obtained, as detailed in table 2.

Additionally to this estimated uncertainty based on the model function, there may exist some other uncertainty components missed in our evaluation. An example can be the uncertainty due to the non-repeatability of the irradiance measurements $u_{NR}(E)$ performed by the radiometer. This non-repeatability is not necessarily associated to the stability or noise of the voltage measurements (that is actually included into the uncertainty of V_{TE}, V_{TS}) but of the entire AHF system as a whole. This non-repeatability component u_{NR} is difficult to calculate during normal outdoor operation, because usually only individual irradiance values E_i are periodically determined by AHF at regular intervals (without averaging a set of DNI values taken in series). An estimate of this $u_{NR}(E)$ uncertainty could be obtained by a laboratory experiment in which a stable white source (e.g. a 1000 W FEL lamp) be repeatedly measured by the radiometer [75]. Alternatively, a rough $u_{NR}(E)$ contribution could also be inferred from the standard deviation σ values shown by our AHF radiometer during the past IPCs when compared to WSG ($\sigma = 629 \times 10^{-6}$ with $N = 280$ in IPC-XII [30], $\sigma = 674 \times 10^{-6}$ with $N = 422$ in IPC-XI [76]). Considering these results, a relative pooled estimate of $u_{NR}(E)/E$ would be: $\sigma/\sqrt{N} \approx 35 \times 10^{-6}$, which is negligible in comparison to the obtained $u_C(E)/E$.

The optical quality factor γ in table 2 is the only term still based on the data provided by the manufacturer. Similarly to L factor, there is a lack of specific details about how this value of γ and its uncertainty were obtained (probably, it was calculated by Hickey and Frieden for the HF original versions [41, 46] but it was not published). Estimation of γ by numerical computation and by additional experiments is currently underway, and upcoming results will be presented in a future work in which optical characterization of AHF and PMO6 radiometers will be analysed in detail. Preliminary results [65] are in good agreement with the value of γ included in table 2 so it has been considered valid enough for the purpose of the evaluation of the uncertainty in this moment.

5. Discussion

As shown, with the exception of the optical factor γ, the input quantities in the AHF MMF have been fully characterized with its associated uncertainty. Many other complementary tests for in-deep knowledge of the sensor, the control electronics and the system operation as a whole have also been carried out, although not described in this work. But, despite the effort put into the characterization of AHF, even with a deeper knowledge of the instrument and the improvements achieved, there are some aspects that still need to be studied and analysed further.

As it can be seen in table 2, combined uncertainty is mainly affected by the non-equivalence factor L and by the voltage signals V_{TE}, V_{TS}. All other terms are negligible when compared to these ones. Coincidently, as suggested above, these large contributions are affected by the uncertainty associated

Table 2. Evaluation of the uncertainty contributions and sensitivity coefficients, according to equation (15).

Term	Estimate/test value	Uncertainty ($k = 1$)	Sensitivity coefficient	Contribution ($\times 10^{-6}$)	Relative contribution
L	1.000 135	0.002 384	0.999 86	2383.4	31.84%
A	50.183 mm^2	0.0075 mm^2	1992.7 m^{-2}	149.5	0.13%
α_C	0.999 12	0.000 06	1.0009	61.2	0.02%
γ	1.001[a]	0.0005[a]	0.9990	500.0	1.40%
V_{TE}	0.956 152 mV	0.002 344 mV	1045.2 V^{-1}	2449.8	33.64%
V_{TS}	0.966 129 mV	0.002 344 mV	1034.4 V^{-1}	2424.9	32.96%
V_{T0}	−0.624 680 μV	0.002 310 mV	10.786 V^{-1}	24.9	0.00%
V_H	2.508 384 V	0.080 751 mV	0.398 84 V^{-1}	32.2	0.01%
V_I	0.166 645 V	0.008 069 mV	5.9981 V^{-1}	48.4	0.01%
R_C	50.9907 mΩ	0.003 37 mΩ	6.6464 mΩ^{-1}	0.022	0.00%
R_N	9.998 69 Ω	0.054 99 mΩ	99.956 mΩ^{-1}	5.5	0.00%
—	—	Total $u(E)/E$	($k = 1$)	4224	100.0%

[a] The value of γ is the originally given by the manufacturer.

to the thermopile output measured by the 34970A data-logger. Therefore, there could be a correlation between values of L and those of (V_{TE}, V_{TS}, V_{T0}) not considered in equations (13) and (14) or even a possible double computation of uncertainties among $L(k_S, k_E)$ and (A, V_{TE}, V_{TS}, V_{T0}, R_N, R_C).

Reduction of the uncertainty contributions of V_{TE}, V_{TS} is a question of major importance, which could probably be achieved through the use of a different voltmeter. The Agilent 34970A seems quite adequate for measuring the rest of operational variables (V_H, V_I and temperatures), but not for the small thermopile signals (∼1 mV and below). A new micro-voltmeter specific for these readings, with a better match between the range or full scale value and the signals, and enhanced resolution and accuracy, would be required.

The other issue to review is the proposed method for determination of L. Although, in theory, the method could be suitable, the current procedure makes the irradiance measured by AHF to be dependent on a particular radiant source (Sun) and on the reference standard determining its radiant power (WSG). In order to consider the radiometer as absolute, it is supposed it should be independent from the WSG that is the reference standard used for the calibration by comparison (in figure 1), even though that reference is only used in our case for evaluation of the k_S slope. Moreover, value of k_E would be traceable to SI units while k_S would be traceable to WRR, so the mentioned 0.3% shift between scales could be affecting the value of L as a spurious contribution. The question is also how independent the determinations of k_E and k_S have to be from each other (that is, if separate experiments with different instrumentation and standards are required or not). Therefore, the method would need to be further developed and improved to clarify these aspects.

In this sense, a first comparison of AHF irradiance against trap detectors and/or cryogenic radiometers of the SI lab scale, in collaboration to IO-CSIC (DI of the Spanish NMI, CEM, for radiometry quantities), is going to be carried out. This will serve to verify if a different value of L is found or not, and to evaluate the validity of the method. It would also be convenient to look for alternative methods of determining L (also with the goal of reducing uncertainty), for example, through dedicated experiments in a vacuum chamber to evaluate the effect of air convection. Whenever possible, these alternative methods should also avoid making L dependent on other parameters in the model function (such as A, R_N, R_C). However, although the method could require supplementary refinements or modifications, we consider it to be valuable in understanding how the *Principle of Equivalence* is materialized in practice in the AHF radiometer.

Besides these lines of work, the total uncertainty attainable for AHF through characterization is an open question. The *ab initio* hypothesis of this research was that something below $U \leqslant 1000 \times 10^{-6}$ ($k = 2$) could be a reasonable goal. The current figure for the standard uncertainty of 4224×10^{-6} ($k = 1$) is clearly larger than desired. Reaching such an uncertainty level needs all the individual uncertainty contributions to be below that figure and their sensitivity coefficients to be small enough too. The introduction of a suitable micro-voltmeter could reduce the V_{TE}, V_{TS} contributions up to $\sim 50 \times 10^{-6}$, which would create a significant improvement to the voltage uncertainties. Revision of some concepts and procedures, as well as estimation of uncertainties obtained through simulation programs, can aid in refining the current contributions of other input quantities. Thus, based on the experience gained in this research, it seems that goal of uncertainty can be achieved in the near future.

Most importantly, the traceability of the AHF to both WRR and SI scales after the characterization has to be analysed. For comparison purposes, the WRR factor obtained by this AHF during last IPC-XII (2015) [30] was of $F_{WRR} = 0.997\ 318$, stable with respect to the previous value of $F_{WRR} = 0.997\ 308$ obtained in IPC-XI (2010) [76]. These factors indicate that the AHF instrument measures DNI values around a 0.27% higher (≈1/0.9973) than WSG before applying the correction. Additionally, the uncertainty of our AHF for the transference of WRR scale to Class A pyrheliometers (outdoor calibration by comparison) is $U = 2264 \times 10^{-6}$ ($k = 2$) [36]. These relative factors and uncertainties have been represented in figure 9, as well as those of WRR and SI reference scales. As commented

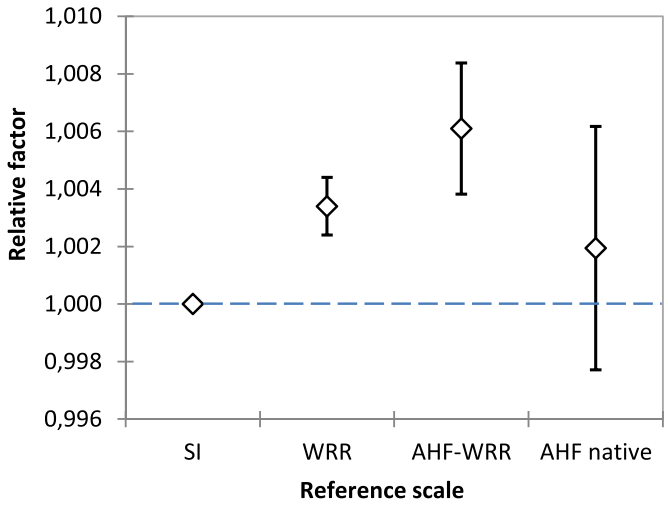

Figure 9. Comparison among AHF equivalent factors and uncertainties on different scales, as explained in the text.

in the introduction, the WRR scale is shifted 0.34% above SI and the attributed uncertainty to WRR is of 0.3% ($k = 3$) [32, 34]. An SI lab scale can be realized with uncertainties of 0.01% [32] or probably better.

The current value for the AHF in its native scale is also represented in figure 9, after the results shown in this work. The shift of 0.41% from the AHF–WRR value is obtained by only considering the change in the L, A and α_C parameters during characterization with respect to their original values used during past IPCs (C_F changes from 20 010 m^{-2} to 19 927 m^{-2}). As it can be seen graphically, the resulting uncertainty is obviously large, but the correction factor obtained up to now clearly shows the progress achieved in the characterization of this instrument towards its alignment with SI lab scale. Apart from the aspects to be improved in the characterization, mentioned above, additional input quantities into the model function (such as a diffraction term, not considered previously for AHF in the literature) could also help in reducing the existing gap. Additional finer corrections in I_H and P_E (thanks to the calibrated values of R_C and R_N, and its temperature dependence) could also improve the result.

6. Conclusions

In this work, a general procedure for the characterization of solar-type ACRs, as a means of obtaining direct traceability to SI, has been described. The method is based on the MMF of the radiometers, which serves to identify input quantities requiring calibration and/or simulation and to calculate the uncertainty budget for the instrument.

The focus has been put on the description of specific calibrations, computation and modelling used for the estimation of the parameters and physical magnitudes in the measurement function of the Eppley Labs' AHF radiometer. In some cases, fundamental advances have been produced thanks to the use of procedures for the determination of parameters (and their uncertainties) that are not well documented in the literature nor in the datasheet of the instrument.

A new method for the computation of the non-equivalence factor L based on the materialization of the *Principle of Equivalence* in the AHF radiometer, has been proposed, obtaining values consistent with the original one given by the manufacturer. The method has been critically reviewed in order to point out its deficiencies and the aspects needing further development. As seen, current procedure would not meet the requirements for an absolute instrument.

The method for calibration of the area of the precision apertures has been improved for reducing its uncertainty up to 0.03% ($k = 2$), by direct computation of the area instead of using the radius of the circumference. The effective absorptance α_C of the cavity, considering the reflectance properties of the Z302 paint and the geometry of the cavity, has been determined with an uncertainty as low as $\sim 60 \times 10^{-6}$. Results from the calibration of the shunt resistor R_N, used for the measurement of the current into the heater of the cavity, and of the parasitic resistance R_C of the wires connecting the cavity, have been also reported. Additionally, care characterization of the temperature dependence of R_N, thanks to the addition of a resistance thermometer into the control box close to this shunt resistor, will now allow introducing finer corrections in the calculation of the solar irradiance.

The combined effect of these results, as a whole, implies a decrease of around 0.4% in the irradiance values measured by AHF, which is larger than the 0.27% of difference with respect to WRR found for this instrument in the two last (IPC-XI and IPC-XII), and approaches the native AHF scale to the SI lab scale. Additional details for reducing the gap towards that SI scale have also been suggested.

The detailed uncertainty calculation has produced a value of the standard uncertainty $u = 4224 \times 10^{-6}$ as result, which is $\sim$8 times larger than the initial goal of an expanded uncertainty $U = 1000 \times 10^{-6}$ ($k = 2$) of this research. Main contributions to uncertainty have been identified as coming from the datalogger used for the measurements of thermopile output signals, as well as from the L factor. Alternative instrumentation (a new nano/micro-voltmeter) and a different method for computation of L have been pointed out as needed for progressing in the characterization of the instrument and in the reduction of the uncertainty.

As a final remark, according to these results and the expected improvements in the future, the objectives of getting traceability of solar irradiance to SI units and of reducing the expanded uncertainty below the desired threshold of $U = 0.1\%$ ($k = 2$) seem to be achievable.

Data availability statement

All data that support the findings of this study are included within the article (and any supplementary files).

Acknowledgments

Authors thank F J Ibañez (CIEMAT) for his support in the development of the 3D models of the AHF radiometer.

This work has partially been supported by the Spanish Ministry of Science and Innovation, National Funding Program for Scientific and Technical Research of Excellence, Generation of Knowledge subprogram, 2017 call, 'DEPRISACR' Project (reference CGL2017-87299-P).

Final note

References to commercial equipment, instruments, or materials in this paper are only given for descriptive purposes, in order to explain adequately the procedures applied. Such references are neither intended to imply recommendation or endorsement by any of our companies (CIEMAT, INTA, CEM), nor qualification about the quality of the equipment.

ORCID iDs

J L Balenzategui https://orcid.org/0000-0002-1057-8450
J de Lucas https://orcid.org/0000-0001-9030-6721
J Cuenca https://orcid.org/0000-0003-0691-2396
A González-Leiton https://orcid.org/0000-0002-5088-2553
M Molero https://orcid.org/0000-0001-5549-7956
F Fabero https://orcid.org/0000-0001-7019-7417
J P Silva https://orcid.org/0000-0002-3133-4973
E Prieto https://orcid.org/0000-0001-5957-5501

References

[1] Arias P A *et al* Climate change 2021: the physical science basis. contribution of working group I to the sixth assessment report of the Intergovernmental panel on climate change (available at: www.ipcc.ch/report/sixth-assessment-report-working-group-i/) (Accessed January 2022)
[2] Fox N, Kaiser-Weiss A, Schmutz W, Thome K, Young D, Wielicki B, Winkler R and Woolliams E 2011 Accurate radiometry from space: an essential tool for climate studies *Phil. Trans. R. Soc.* A **369** 4028–63
[3] World Meteorological Organization 2016 The global observing system for climate: implementation needs WMO/GCOS-200 Report
[4] World Meteorological Organization 2011 Systematic observation requirements for satellite-based data products for climate WMO/GCOS-154 Report
[5] Ohring G B, Wielicki B, Spencer R, Emery B and Datla R 2005 Satellite instrument calibration for measuring global climate change: report on a workshop *Bull. Am. Meteorol. Soc.* **86** 1303–13
[6] Gueymard C A 2018 A reevaluation of the solar constant based on a 42-year total solar irradiance time series and a reconciliation of spaceborne observations *Sol. Energy* **168** 2–9
[7] Kopp G and Lean J L 2011 A new, lower value of total solar irradiance: evidence and climate significance *Geophys. Res. Lett.* **38** L01706
[8] Coddington O, Lean J L, Pilewskie P, Snow M and Lindholm D 2016 A solar irradiance climate data record *Bull. Am. Meteorol. Soc.* **97** 1265–82
[9] Murdock T L and Pollock D B 1998 High accuracy space based remote sensing requirements Report NIST GACR pp 98–748
[10] Pollock D B, Murdock T L, Datla R U and Thompson A 2000 Radiometric standards in space: the next step *Metrologia* **37** 403
[11] Ohring G (ed) 2007 Achieving satellite instrument calibration for climate change (ASIC3) (available at: www.star.nesdis.noaa.gov/star/documents/ASIC3-071218-webversfinal.pdf) (Accessed January 2021)
[12] Frölich C 1991 History of solar radiometry and the World Radiometric Reference *Metrologia* **28** 111–5
[13] Marchgraber R M 1970 The development of standard instruments for radiation measurements *Meteorological Observations and Instrumentation* (*Meteorological Monographs* vol 11) ed S Teweles and J Giraytys (Boston, MA: American Meteorological Society) pp 302–14
[14] Coulson K L 1975 *Solar Terrestrial Radiations. Methods and Measurements* (New York: Academic)
[15] Vignola F, Michalsky J and Stoffel T 2012 Solar and infrared radiation measurements *Energy and the Environment* (USA: CRC Press)
[16] Stanhill G and Achiman O 2017 Early global radiation measurements: a review *Int. J. Climatol.* **37** 1665–71
[17] Balenzategui J L, Fabero F and Silva J P 2019 *Solar Resources Mapping* ed J Polo, L Martin-Pomares and A Sanfilippo (Berlin: Springer) pp 15–69
[18] World Meteorological Organization CIMO 1977 Abridged final report of the seventh session WMO Report No. 490—Annex IV
[19] Frölich C and London J 1986 Revised instruction manual on radiation instruments and measurements World Climate Research Programme Publications Series No. 7. WMO/TD Report No. 149
[20] Haley F, Kendall J M and Plamondon J 1965 Cavity type radiometer for absolute total intensity measurement of visible and IR radiation *Proc. 11th National Aerospace Instrumentation Symp.* vol 1 (ISA) pp 3–65
[21] Kendall J M 1968 The JPL standard total-radiation absolute radiometer *JPL Technical Report* pp 32–7263
[22] Dewitte S and Clerbaux N 2017 Measurement of the earth radiation budget at the top of the atmosphere—a review *Remote Sens.* **9** 1143
[23] Zerlaut G A 1982 Solar radiation measurements: calibration and standardization efforts *Advances in Solar Energy* vol 1, ed K W Boer and J A Duffie (Boulder, CO: American Solar Energy Society) pp 19–60
[24] 1976 *Fourth Int. Pyrheliometer Comparisons—third regional pyrheliometer comparisons (RA VI) (6–24 October 1975)* World Radiation Center Davos Swiss Meteorological Institute, Working Report No. 58
[25] Estey R S and Seaman C H 1971 Four absolute cavity radiometer (pyrheliometer) intercomparisons at New River, Arizona JPL Publication 81-60 (Jet Propulsion Laboratory)
[26] World Meteorological Organization CIMO Guide 2017 WMO guide to meteorological instruments and methods of observation Report WMO-No. 8
[27] ISO International Standard ISO9060:2018 Solar energy—specification and classification of instruments for measuring hemispherical solar and direct solar radiation
[28] Fox N P and Rice J P 2005 *Optical Radiometry* ed A C Parr, R U Datla and J L Gardner (Amsterdam: Elsevier) pp 35–96
[29] Hengstberger F 1989 *Absolute Radiometry* (New York: Academic)
[30] Finsterle W 2016 Final report of the WMO International Pyrheliometer Comparison IPC-XII (2015) WMO IOM Report No. 124
[31] Romero J, Fox N P and Fröhlich C 1991 First comparison of the solar and an SI radiometric scale *Metrologia* **28** 125–8

[32] Romero J, Fox N P and Fröhlich C 1995 Improved comparison of the World Radiometric Reference and the SI radiometric scale *Metrologia* **32** 523–4

[33] Finsterle W, Blattner P, Moebus S, Rüedi S, Wehrli C, White M and Schmutz W 2008 Third comparison of the World Radiometric Reference and the SI radiometric scale *Metrologia* **45** 377–81

[34] Fehlmann A, Kopp G, Schmutz W, Winkler R, Finsterle W and Fox N 2012 Fourth World Radiometric Reference to SI radiometric scale comparison and implications for on-orbit measurements of the total solar irradiance *Metrologia* **49** S34–8

[35] IEC 60904-4:2019 Standard 'photovoltaic devices—part 4: photovoltaic reference devices—procedures for establishing calibration traceability' (International Electrotechnical Commission)

[36] Balenzategui J L, Molero M, Silva J P, Fabero F, Cuenca J, Mejuto E and de Lucas J 2022 Uncertainty in the calibration transfer of solar irradiance scale: from absolute cavity radiometers to standard pyrheliometers *Solar* **2** 158–85

[37] Brusa R W and Fröhlich C 1986 Absolute radiometers (PMO6) and their experimental characterization *Appl. Opt.* **25** 4173

[38] NIST/SEMATECH e-handbook of statistical methods (https://doi.org/10.18434/M32189)

[39] OIML V 2-200 Edition 2007 *International Vocabulary of Metrology—Basic and General Concepts and Associated Terms (VIM)* 3rd edn (Organisation Internationale de Métrologie Légale)

[40] Kendall J M 1968 NASA—JPL Technical Report 32-7263

[41] Hickey J R, Frieden R G, Griffin F J, Cone S A, Maschhoff R A and Gniady J 1977 The self-calibrating sensor of the eclectic satellite pyrheliometer (ESP) program *Proc. Int. Solar Energy Society Annual Meeting* pp 15–1

[42] Willson R C 1973 Active cavity radiometer *Appl. Opt.* **12** 810

[43] Hickey J R and Karoli A R 1974 Radiometric calibrations for the earth radiation budget experiment *Appl. Opt.* **13** 523

[44] Willson R C 1979 Active cavity radiometer type IV *Appl. Opt.* **18** 179

[45] Willson R C 1980 Active cavity radiometer type V *Appl. Opt.* **19** 3256

[46] Crommelynck D A 1982 Fundamentals of absolute pyrheliometry and objective characterization *Earth Radiation Science Seminars* vol 2239 (NASA Conference Publication) p 53

[47] Karoli A R, Hickey J R and Frieden R G 1983 Self-calibrating cavity radiometers at the Eppley laboratory: capabilities and applications *Proc. SPIE* **0416** 43–50

[48] Sapritskii V I and Pavlovich M N 1989 Absolute radiometer for reproducing the solar irradiance unit *Metrologia* **26** 81

[49] Morozova S P, Sapritsky V I and Pavlovich M N 1991 Utilization of absolute radiometers in USSR national standards of irradiance units *Metrologia* **28** 117

[50] Wei F and Xifeng J 1992 Development of a compensate dual-conical cavity absolute radiometer *Acta Energ. Sol. Sin.* **13** 406–11

[51] Wei F, Bingxi Y, Haishun Y, Yu A, Chenghu G and Zhe L 2003 Development of STIM *Proc. SPIE* **4895** 218–24

[52] Kopp G, Heuerman K and Lawrence G 2005 The total irradiance monitor (TIM): instrument calibration *Sol. Phys.* **230** 111–27

[53] Kopp G and Lawrence G 2005 The total irradiance monitor (TIM): instrument design *Sol. Phys.* **230** 91–109

[54] Wei F, Hongrui W, Huiduan L and Yupeng W 2014 Total solar irradiance monitor for Chinese FY-3A and FY-3B satellites–instrument design *Sol. Phys.* **289** 4711–26

[55] Fehlmann A 2011 Metrology of solar irradiance *PhD Thesis* University of Zurich

[56] Suter M 2014 Advances in solar radiometry *PhD Thesis* University of Zurich

[57] Walter B *et al* 2017 The CLARA/NORSAT-1 solar absolute radiometer: instrument design, characterization and calibration *Metrologia* **54** 674–82

[58] Rainer W 2013 Cryogenic solar absolute radiometer. A potential SI standard for solar irradiance *PhD Thesis* University College London (https://doi.org/10.1097/TA.0b013e31829c7b0c)

[59] Reda I 1996 Calibration of a solar absolute cavity radiometer with traceability to the World Radiometric Reference Report NREL/TP 463-20619

[60] Patrick H J, Germer T A, Zarobila C J, Cooksey C C and Yoon H W 2016 Optical reflectance of pyrheliometer absorption cavities: progress toward SI-traceable measurements of solar irradiance *Appl. Opt.* **55** 6346–54

[61] Taylor P, Kipphardt H and de Bièvre P 2001 The definition of primary method of measurement (PMM) of the 'highest metrological quality': a challenge in understanding and communication *Accred Qual. Assur.* **6** 103–6

[62] See reference [18]—Annex V

[63] BIPM, IEC, IFCC, ISO, IUPAC, IUPAP and OIML 2008 *Evaluation of Measurement—Data Guide to the Expression of Uncertainty in Measurement JCGM 100:2008 (GUM 1995 with Minor Corrections)* 1st edn (Sèvres: BIPM Joint Committee for Guides in Metrology)

[64] Balenzategui J L *et al* 2020 Caracterización de radiómetros absolutos de cavidad como patrones primarios de irradiancia solar *CIES2020: As Energias Renováveis na Transição Energética: Livro de Comunicações do XVII Congresso Ibérico e XIII Congresso Ibero-americano de Energia Solar* ed H Gonçalves and M Romero (Lisboa: LNEG) pp 935–42

[65] Balenzategui J L *et al* 2021 On the characterization of an AHF cavity radiometer and its traceability to WRR/SI *IPC-XIII Symp.* (*Davos, Switzerland*, *27 September–15 October 2021*)

[66] Estey R S and Seaman C H 1981 Four absolute cavity radiometer (pyrheliometer) lntercomparisons at New River, Arizona (Jet Propulsion Laboratory Publication) pp 81–60

[67] World Meteorological Organization 1981 *5th Int. Pyrheliometer Comparisons and Absolute Radiometer Comparisons (IPC V), Results and Symp.* (Swiss Meteorological Institute) Working Report No. 94

[68] World Meteorological Organization CIMO 1985 Abridged final report of the ninth session WMO Report No. 651

[69] World Meteorological Organization 1991 *Int. Pyrheliometer Comparisons (IPC VII), Results and Symp.* (Swiss Meteorological Institute) Working Report No. 162

[70] (Example of physical properties are available at: www.nealloys.com/36_alloy_invar.php) (Accessed February 2022)

[71] Neugebauer M, Schulz D and Krystek M 2015 Calibration of circular apertures using an optical CMM *Proc. Euspen's 15th Int. Conf. & Exhibition* (*Leuven, Belgium*) pp 153–4

[72] BIPM, IEC, IFCC, ISO, IUPAC, IUPAP and OIML 2008 Evaluation of measurement data, supplement 1 to the 'guide to the expression of uncertainty in measurement' propagation of distributions using a Monte Carlo method JCGM 101:2008 1st edn (BIPM Joint Committee for Guides in Metrology)

[73] Bedford R E and Ma C K 1974 Emissivities of diffuse cavities: isothermal and nonisothermal cones and cylinders *J. Opt. Soc. Am.* **64** 339–49
[74] Preston-Thomas H 1990 The International Temperature Scale of 1990 (ITS-90) *Metrologia* **27** 107
[75] Rodriguez-Outon I, Balenzategui J L, Fabero F and Chenlo F 2010 Characterization of light sources with absolute cavity radiometers for indoor reference solar cell calibration methods *Proc. 25th European Photovoltaic Solar Energy Conf. and Exhibition* (*Valencia, Spain*) pp 549–53
[76] Finsterle W 2011 Final report of the WMO International Pyrheliometer Comparison IPC-XI (2010) WMO IOM Report No. 108